FINAL REPORT

The main goal of the project, "Asymptotically Optimal, High-Order Accurate Algorithms for the Solution of Certain Elliptic PDE's" (DE-FG02-03ER25577) was to develop fast, high-order algorithms for the solution of *scattering problems* and *spectral problems* of photonic crystals theory. The results we obtained lie in three areas: (1) asymptotically fast, high-order algorithms for the solution of **eigenvalue problems of photonics,** (2) fast, high-order algorithms for the solution of **acoustic** and electromagnetic **scattering** problems in the inhomogeneous media, and (3) inversion formulas and fast algorithms for the **inverse source** problem for the acoustic wave equation, with applications to thermo- and opto- acoustic tomography.

1 Eigenvalue problems of photonics

Solution of **eigenvalue problems of photonics** is required for accurate modeling of photonic band-gap materials (photonic crystal structures). Due to the wealth of potential applications of such materials and very high cost of their experimental manufacturing this research is of significant practical interest. The most remarkable property of photonic crystal structures is the existence of spectral gaps arising due to multiple reflections of propagating waves. Opening of spectral gapes is, in particular, a consequence of high-contrast material interfaces in such structures. However, from a computational point of view, sharp interfaces represent considerable difficulties as they lead to singularities of the field derivatives across material boundaries.

In order to model photonic structures with high accuracies required by the modern engineering practice, one has to resort to spectrally accurate algorithms. Our first goal is to design fast, high order solvers for the solution of 2-D spectral problems. 2-D case refers to wave propagation in $x-y$ plane through a structure homogeneous in the z-direction. In order to determine spectral bands and band gaps of a 2-D photonic crystal one has to solve two sets of eigenvalue problems (corresponding to TE and TM polarizations of the EM waves). The first set of these problems is a family of eigenvalue problems for the Poisson equation

$$-\frac{1}{\varepsilon(x)}\Delta u(x) = \lambda u(x), \tag{1}$$

where function $u(x)$ is defined on a rectangular fundamental domain Ω, subject to quasiperiodic boundary conditions

$$u(1,x_2) = u(0,x_2)e^{ik_1}, \quad u(x_1,1) = u(x_1,0)e^{ik_2}. \tag{2}$$

For each value of the quasimomentum $\mathbf{k} =(k_1,k_2) \in [0,\pi]\times[0,\pi]$ problem (1) has a discrete spectrum $\sigma^{Poisson}(\mathbf{k})$. The total (continuous) $\sigma^{Poisson}_{total}$ spectrum of the operator $-\frac{1}{\varepsilon(x)}\Delta u(x)$ is obtained as the union of values $\sigma^{Poisson}(\mathbf{k})$:

$$\sigma^{Poisson}_{total} = \bigcup_{\mathbf{k}\in[0,\pi]\times[0,\pi]} \sigma^{Poisson}(\mathbf{k}).$$

The second set is the eigenvalue problems for the divergence equation

$$-\mathrm{div}\left(\frac{1}{\varepsilon(x)}\nabla v(x)\right) = \lambda v(x), \tag{3}$$

subject to quasiperiodic boundary conditions of the form (2). This operator also has a discrete spectrum $\sigma^{div}(\mathbf{k})$ for each fixed value of the quasimomentum (k_1,k_2), and the total spectrum is

again the union of values over all quasimomenta

$$\sigma_{total}^{div} = \bigcup_{\mathbf{k}\in[0,\pi]\times[0,\pi]} \sigma^{div}(\mathbf{k}).$$

Finally, the full spectrum of the photonic structure σ_{Full} is the union of the spectra of the two operators

$$\sigma_{Full} = \sigma_{total}^{Poisson} \bigcup \sigma_{total}^{div}.$$

We consider a particular, practically important case when dielectric permittivity is piece-wise constant on Ω, i.e. $\varepsilon(x) = \varepsilon_i$ on given subdomains Ω_i of Ω.

Our general approach to numerical solution of these eigenvalue problems relies on Arnoldi iterations of the inverse operators (whose computation is equivalent to the solution of the Poisson and divergence equations with given right hand sides). The advantage of such approach is that the lower eigenvalues of the differential operators (that are of practical interest) become the largest eigenvalues of the inverse (compact) operators, which significantly simplifies their numerical computation. The Arnoldi iterations are organized by calls to ARPACK - one of the most advanced of currently available eigenvalue solvers. The accuracy and efficiency of this approach depends on our ability to solve the Poisson and the divergence equations in fast, high-order fashion.

In order to obtain such fast and accurate solutions we resort to a sort of domain decomposition technique. Namely, in order to solve Poisson equation

$$-\Delta u(x) = \varepsilon(x) f(x), \tag{4}$$

we first obtain a highly accurate solution $u_1(x)$ of this equation equation in a thin domain containing the material interface, by conformally mapping it onto an annulus, and by solving the Poisson equation in this new domain by fast pseudospectral method based on combined Chebyshev/Fourier approximations. Due to our choice of the conforming computational grids, we are able to accurately model jump conditions across the interfaces. Next, the solution $u_1(x)$ in the interface region is multiplied by a C_0^∞ function $\eta(x)$ vanishing on the boundary of that region together with its higher derivatives:

$$u_1^*(x) = \eta(x) u_1(x).$$

Finally, we solve auxiliary Poisson equation

$$-\Delta u_2(x) = \varepsilon(x) f(x) - \Delta u_1^*(x) \tag{5}$$

and, thus, obtain the solution $u(x) = u_1^*(x) + u_2(x)$ of equation (4). This allows us to reduce the solution of the Poisson equation (4) with a discontinuous right hand side, to equation (5) with a smooth right hand side, which is easily and accurately computed using standard Fourier decomposition techniques.

In turn, in order to solve the divergence equation

$$-\mathrm{div}\left(\frac{1}{\varepsilon(x)}\nabla v(x)\right) = f(x), \tag{6}$$

I utilize the fact that the underlying material coefficient is piece-wise constant. This permits the reduction of the problem to the solution of the Poisson equation in the subdomains. The subdomain solutions are subsequently glued together by adding a harmonic function with required jumps on the boundaries of the subdomains.

The numerical experiments with material configurations containing smooth boundaries of general shape demonstrate high-order convergence for both eigenvalue problems. A typical example

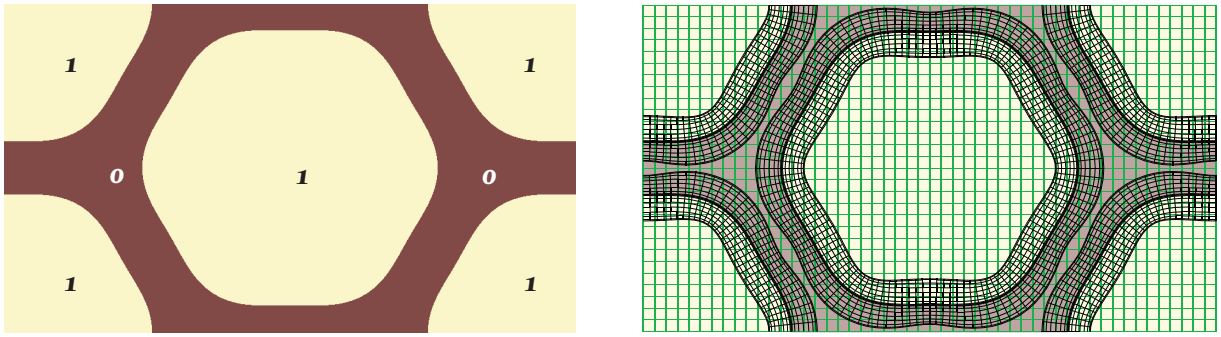

(a) (b)

Figure 1: (a) Hexagonal structure (b) Computational grids

of such computation is briefly described below. The "smooth hexagonal" material configuration is represented by the fundamental cell in Figure 1(a), with $\varepsilon_0 = 10, \quad \varepsilon_1 = 1$. Figure 1(b) shows the combination of overlapping grids we use in the algorithm. Finally, Table 1 presents results of convergence study for the eigenvalues of the divergence equation. The "Relative error" column represents maximum relative error in each of the first thirty eigenvalues. Value of the errors were obtained by comparison with the most accurate of the runs that was performed on a grid 720×1296 (not shown in the table). One can clearly see the high-order convergence of the method, and high accuracy of computations that can be obtained using the present approach. Moreover, the com-

Grid size	256×448	360×648	512×896
Relative error	$3.1 \cdot 10^{-7}$	$2.9 \cdot 10^{-9}$	$6.7 \cdot 10^{-11}$

Table 1: Convergence study for the divergence equation

putation times (not shown) grew almost linearly with the number of unknowns in these runs thus confirming asymptotically fast character ($\mathcal{O}(n\log n)$ flops) of our algorithm.

These results were presented at the minisymposium *"Light and Wave Propagation in Inhomogeneous Media: Theory and Modeling"*, SIAM Conference on Mathematical Aspects of Materials Science, LA. May 23-26, 2004. Currently I am preparing this material for publication.

2 Fast, high-order algorithms for scattering problems

2.1 Acoustic scattering

In this section we consider a problem of acoustic scattering from an object with variable speed of sound (or refractive index). The incoming wave $u^{inc}(x)$ impinges on an object with variable refractive index $\varepsilon(x) = 1 - m(x)$ (where $m(x)$ is compactly supported). The scattered field $u^{scat}(x)$ satisfies the radiation boundary conditions

$$\lim_{r\to\infty} \sqrt{r}\left[\frac{\partial u^{scat}(x)}{\partial r} - iku^{scat}(x)\right] = 0, \qquad r = |x|,$$

where k is the wave number of the incoming field, while the total field $u(x) = u^{scat}(x) + u^{inc}(x)$ satisfies the Helmholtz equation

$$\Delta u(x) + k^2(1 - m(x))u(x) = 0. \tag{7}$$

The problem is usually re-formulated in the form of the Lippmann-Schwinger integral equation

$$u(x) = u^{inc}(x) - k^2 \int \Phi(x-y)m(y)u(y)dy, \tag{8}$$

where

$$\Phi(x) = \frac{1}{4\pi}\frac{e^{ik|x|}}{|x|}$$

is the Green's function of the free-space Helmholtz equation satisfying the radiation condition at infinity:

$$\Delta\Phi(x) + k^2\Phi(x) = -\delta(x).$$

One of the most efficient ways to solve the scattering problem is to solve the integral equation of the second kind (8) through application of iterative solvers, such as GMRES. This, in turn, requires multiple computations of a convolutions in the form $C(x) = \int \Phi(x-y)m(y)h(y)dy$.Thus, in order to solve the scattering problem fast and in a high-order fashion one needs be able to compute accurately and fast convolutions of a finitely supported function with the Green's function $\Phi(x)$. This step is challenging due to the singularity of $\Phi(x)$ at $x = 0$. The most advanced of the existing methods either rely on sophisticated techniques, like projections on the space of band-limited functions, or splitting of the Green's function into a sum of the smooth and singular components combined with integrating the singular part in the moving spherical coordinate system. Instead, we propose an extremely fast and accurate method of evaluating such convolutions. Our algorithm utilizes Cartesian grid only, and it does not involve the use of special functions or high-order polynomial interpolation. To accomplish this, we represent the free-space Green's function as a sum of the periodic Green's function $\Phi^{per}(x)$ and a smooth term $\Phi_1(x)$:

$$\Phi(x) = \Phi^{per}(x) + \Phi_1(x),$$

where $\Phi^{per}(x)$ is a periodic solution of the Helmholtz equation

$$\Delta\Phi^{per}(x) + k^2\Phi^{per}(x) = -\delta(x),$$

in a a cube Q (of non-resonant size) containing the support of $m(x)$, and $\Phi_1(x) = \Phi(x) - \Phi^{per}(x)$.Now the desired convolution can be computed as the sum of two terms

$$\begin{aligned} C(x) &= C_1(x) + C^{per}(x), \\ C_1(x) &= \int \Phi_1(x-y)m(y)h(y)dy, \\ C^{per}(x) &= \int \Phi^{per}(x-y)m(y)h(y)dy. \end{aligned}$$

The first term $C_1(x)$ in the above equation is a convolution of a finitely supported $m(x)h(x)$ with a real-analytic function $\Phi_1(x)$. (In the next section we explain how to precompute this function accurately and fast). A convolution with $\Phi_1(x)$ can be computed fast if the functions are represented by their values on a Cartesian grid, by application of the Fast Fourier transform (FFT). Moreover, if $m(x)$ (and therefore, $h(x)$) is smooth, the computation is automatically high-order accurate.

The first term $C^{per}(x)$ can be understood as a periodic solution of the equation

$$\Delta C^{per}(x) + k^2 C^{per}(x) = -m(y)h(y);$$

it can also be easily found by using the FFT. Again, if $m(x)$ is sufficiently smooth, the result is automatically high-order accurate. Equivalently, one can find a band limited version $\Phi^{BL}(x)$ of

$\Phi^{per}(x)$, and compute the convolution $C^{per}(x) \approx \int \Phi^{BL}(x-y)m(y)h(y)dy$ using the FFT. The advantage of this modification is in that the functions $\Phi^{BL}(x)$ and $\Phi_1(x)$ can be added, so that the whole convolution $C(x)$ is approximated by

$$C(x) \approx \int \left[\Phi^{BL}(x-y) + \Phi_1(x)\right] m(y)h(y)dy.$$

If $m(x)$ is discretized on a grid $n \times n \times n$, computation of such a convolution requires only two FFT's of the size $2n \times 2n \times 2n$ (if the Fourier transform of $\left[\Phi^{BL}(x-y) + \Phi_1(x)\right]$ is pre-computed).

2.1.1 Pre-computation of $\Phi_1(x)$

In order to make the algorithm work we need to pre-compute function $\Phi_1(x)$, such that

$$\left[\Delta + k^2\right] \Phi_1(x) = 0, \tag{9}$$

and such that $\Phi(x) - \Phi_1(x)$ is periodic. To this end, let us introduce C_0^∞ function $\eta_0(x)$ vanishing toward the boundaries of the computational domain $Q$with all the derivatives and equal to 1 in the neighborhood of 0, and define $\eta(x) = 1 - \eta_0(x)$. Compute

$$w(x) = \left[\Delta + k^2\right] (\eta(x)\Phi(x));$$

this can be easily done analytically if $\eta_0(x)$ is selected to be a radial function. Now, function $w(x)$ is compactly supported C_0^∞ function (equal 0 in the neighborhood of 0 and in the neighborhood of the cube's boundary ∂Q). By utilizing the FFT find the periodic solution $W(x)$ of the equation

$$\left[\Delta + k^2\right] W(x) = -w(x).$$

Due to the smoothness of $w(x)$ such a computation is high-order accurate. Compute $\Phi_1(x)$ as

$$\Phi_1(x) = W(x) + \eta(x)\Phi(x).$$

It is easy to check that so computed $\Phi_1(x)$ indeed satisfies equation (9). On the other hand, in the neighborhood of ∂Q, the difference $\Phi(x) - \Phi_1(x)$ equals to $-W(x)$, and is, therefore, periodic.

2.1.2 The case of non-smooth scatterers

2.1.3 Numerical results

The above algorithm is extremely simple, it involves only calls to the Fast Fourier transform routines and simple arithmetical operations. Importantly, the present method is spectrally accurate for smooth $m(x)$. A simple convergence study below illustrates the high-order nature of this algorithm for an infinitely smooth $m(x)$. Table 2 shows maximum error in the magnitude of the far field versus the grid size.

Grid size	Number of unknowns	Error
256×256	65536	$2 \cdot 10^{-4}$
512×512	262144	$5.7 \cdot 10^{-6}$
1024×1024	1048576	$1.2 \cdot 10^{-8}$

Table 2: Convergence study for the Helmholtz equation, smooth scatterer, 2-D

This simple Helmholtz solver will not yield high-order convergence when applied to discontinuous $n(x)$. In this case a good accuracy of computations is achieved if one replaces discontinuous $n(x)$ by its band-limited version $n^{BL}(x)$, with the cut-off frequency equal to the Nyquist frequency of the discretization grid. We illustrate this technique by computing acoustic scattering from a penetrable sphere in 3-D, with $kR = 20$ (where k is the wavenumber, and R is the radius of the sphere). The incoming wave propagates in x-direction, i.e. from the left to the right. We compare the results with the exact solution represented by the Mie series. As one can conclude from the table, the method exhibits, roughly, a third order convergence.

Grid size	Number of unknowns	Time per it, sec.	Rel. error
$64 \times 64 \times 64$	262144	1.6	$6 \cdot 10^{-2}$
$128 \times 128 \times 128$	2097152	20	$3 \cdot 10^{-3}$
$256 \times 256 \times 256$	16777216	140	$7 \cdot 10^{-4}$

Table 3: Convergence study for the Helmholtz equation; scattering from a sphere with $kR = 20$

The gray-scale plot of the total field $u(x)$ for this sphere is shown in the Figure below.

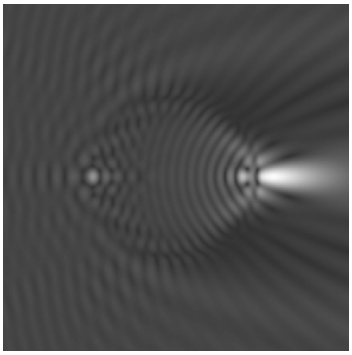

Figure 2: Acoustic scattering from a sphere in 3-D, $kR = 20$, total field, central cross-section

2.2 Electromagnetic scattering

The propagation of time-harmonic electromagnetic waves through inhomogeneous medium is governed by the Maxwell equations

$$\nabla \times E = ikH \tag{10}$$

$$\nabla \times H = -ikn(x)E \tag{11}$$

where the wavenumber k is defined as $k^2 = \varepsilon_0 \mu_0 \varpi^2$, ϖ is the frequency, ε_0 and μ_0 are the electric permittivity and magnetic permeability of the surrounding medium. The refractive index $n(x)$ is defined as

$$n(x) = \frac{1}{\varepsilon_0} \left(\varepsilon(x) + i \frac{\sigma(x)}{\varpi} \right),$$

where $\varepsilon(x)$ and $\sigma(x)$ are the electric permittivity and conductivity of the scatterer.

2.2.1 Electric field equation

In order to compute scattering of an electromagnetic wave from an inhomogeneous penetrable object one can solve the electric field integral equation

$$E(x) = E^{inc}(x) - k^2 \int \Phi(x-y) m(y) E(y) dy + \operatorname{grad}_x \int \frac{1}{n(y)} \operatorname{grad} n(y) \cdot E(y) \Phi(x-y) dy, \quad (12)$$

where $m(x) = 1 - n(x)$, E^{inc} is the E-component of the incoming wave, and $\Phi(x)$ is, as in the previous section, the free-space Green's function of the Helmholtz equation. For sufficiently smooth $n(x)$ the above integral equation is a Fredholm equation of the second kind, and iterative methods, such as GMRES, yield good results.

The challenging part, here, as in the acoustic case, is the computation of convolutions with $\Phi(x)$. Indeed, in the case of smooth $n(y)$ equation (12) can be re-written in the form

$$E(x) = E^{inc}(x) - k^2 \int \Phi(x-y) m(y) E(y) dy + \int \operatorname{grad} \left[\frac{1}{n(y)} \operatorname{grad} n(y) \right] \cdot E(y) \Phi(x-y) dy; \quad (13)$$

now the gradients can be efficiently computed using the FFT. In order to compute the convolutions with $\Phi(x)$ we use the method described in the previous section (component-wise). After $E(x)$ has been computed, the magnetic induction H can be calculated from (10), if desired.

If $n(y)$ is discontinuous, so is the second integral in the equation (13) (or (12)). Therefore these equations are no longer proper equations of the second kind (the integral operator is not compact). The remedy for the discontinuous case is to solve the magnetic field equation instead.

2.2.2 Magnetic field equation

The equation for the magnetic field (in case of constant magnetic permeability) can be written in the form:

$$H(x) = H^{inc}(x) - k^2 \int \Phi(x-y) m(y) H(y) dy + \int \left[\frac{1}{n(y)} \operatorname{grad} n(y) \times \operatorname{curl} H(y) \right] \Phi(x-y) dy.$$

For the discontinuous $n(x)$ the second term of this equation behaves similarly to a single layer potential, and is continuous. Both integral operators are compact, even if $n(x)$ is discontinuous, and the equation remains a second kind Fredholm integral equation. Once $H(x)$ has been computed, $E(x)$ can be computed using equation (11).

An example of such computation is described below. The absolute value of y component of the magnetic field scattered by a sphere with the size is presented as a gray scale image in figure 3. The radius of the sphere equals 0.5, the wavenumber equals 10. The incoming wave propagates in z-direction i.e. upward. The number of unknowns was about 50 millions in this numerical experiment, and one iteration took about 525 seconds. The comparison with the exact solution obtained by summing Mie series, shows that the relative local error was of order of $5 \cdot 10^{-3}$.

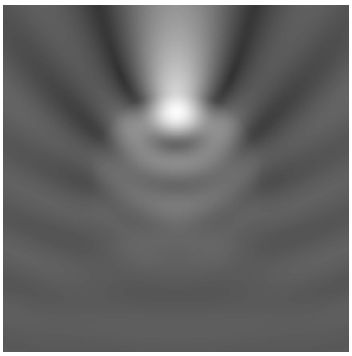

Figure 3: EM scattering from a sphere in 3-D, $kR = 5$, central cross-section of $|H_y(x)|$ is shown

3 Inverse problem for the wave equation

Some of the most practically important applications of asymptotically fast methods in PDEs can be found in inverse problems, in particular in tomography modalities based on wave propagation. Under support of the current grant we have received several important results in the area of the so-called thermoacoustic tomography (TAT). This novel and very promising modality combines the sensitivity (or high contrast) of electromagnetic waves with the high-resolution of traditional ultrasound diagnostics. The measurement procedure starts with a short EM pulse that illuminates the region of interest. (One of the most promising applications, for example, is the mammography, i.e. breast imaging in women). The absorption of the EM energy in tissues causes the thermoacoustic expansion; an acoustic wave starts to propagate. The intensity of the source depends on how much energy is absorbed; it turns out that the absorption in the tumors is significantly higher than in healthy tissues. The wave is measured by the acoustic transducers (or detectors), located on some surface (completely or partially) surrounding the region of interest. If one manages to reconstruct the intensity distribution of the source of US waves from the data measured by the detectors, an important information about possible cancerous tumors is obtained.

Let us denote the speed of sound at location x by $c(x)$. Then, modulo some constant coefficients that we will assume all to be equal to 1, the pressure wave $p(x,t)$ satisfies the following problem for the wave equation:

$$\begin{cases} p_{tt} = c^2(x)\Delta_x p, & t \geq 0, x \in \mathbb{R}^3 \\ p(x,0) = f(x), \\ p_t(x,0) = 0 \end{cases} \tag{14}$$

The goal is to find, using the data measured by transducers, the initial value $f(x)$ at $t = 0$ of the solution $p(x,t)$. A transducer at time t measures the average pressure over its surface at this time, which for the small size of the transducer can be assumed to be just the value of $p(y,t)$ at the location y of the transducer. Dimension count shows immediately that in order to have enough data for reconstruction of the function $f(x)$, one needs to collect data from the transducers' locations y running over a surface S in $\mathbb{R}^3$.

Taking into account that the measurements produce the values $g(y,t)$ of the pressure $p(x,t)$ of (14) on $S \times \mathbb{R}^+$, the set of equations (14) extends to become

$$\begin{cases} p_{tt} = c^2(x)\Delta_x p, & t \geq 0, x \in \mathbb{R}^3 \\ p(x,0) = f(x), & \\ p_t(x,0) = 0 & \\ p(y,t) = g(y,t), & y \in S \times \mathbb{R}^+ \end{cases} \tag{15}$$

The problem now reduces to finding the initial value $f(x)$ in (15) from the knowledge of the lateral data $g(x,t)$. We consider below only the case of constant speed of sound $c(x)$. (This approximation works quite well when only soft tissues are present in the region of interest — as is the case in the breast imaging). We will assume that the units are chosen in such a way that $c(x) = 1$. The known Poisson-Kirchoff formula for the solution of (14) gives

$$p(x,t) = a\frac{\partial}{\partial t}\left(t(Rf)(x,t)\right), \tag{16}$$

where

$$(Rf)(x,r) = \int\limits_{|y|=1} f(x+ry)dA(y) \tag{17}$$

is the *spherical mean operator* applied to the function $f(x)$, dA is the normalized area element on the unit sphere in $\mathbb{R}^3$, and a is a constant. Hence, knowledge of the function $g(x,t)$ for $x \in S$ and all $t \geq 0$ essentially means knowledge of the spherical mean $Rf(x,t)$ at all points $(x,t) \in S \times \mathbb{R}^+$. One thus is led to studying the spherical mean operator $R : f \to Rf$ and in particular its restriction R_S to the points $x \in S$ only (these are the points where we place transducers):

$$h(x,t) \equiv R_S f(x,t) = \int\limits_{|y|=1} f(x+ty)dA(y), \qquad x \in S, t \geq 0. \tag{18}$$

3.1 Inversion formulas

One way of finding $f(x)$ from the known values of its spherical Radon transform $h(x,t)$ is to discretize equation (18) and to solve the resulting linear system using standard linear algebra routines. This approach is not practical, however. Indeed, if the function of a 3-D variable $f(x)$ is represented by its values on a grid of size $n \times n \times n$, the number of unknowns is n^3, and the operation count for the LU decomposition is $\mathcal{O}(n^9)$. This number is, of course, prohibitively large. In the classical modalities, such as X-ray tomography, some of the most efficient and widely used in practice reconstruction techniques are the ones based on explicit inversion formulas for the classical Radon transform. For the spherical Radon transform (18) that is describes the inverse problem in the thermoacoustic tomography, the first set of exact inversion formulas of filtered backprojection type was discovered in [9]. These formulas were obtained only in odd dimensions.

The PI found a set of explicit inversion formulas that work in arbitrary dimensions [3]:

$$f(x) = \frac{1}{4(2\pi)^{n-1}}\mathrm{div}\int\limits_{\partial B} \mathbf{n}(y)H(y,|x-y|)dA(y). \tag{19}$$

Here

$$H(y,t) = \int\limits_{\mathbb{R}^+} \left[Y(\lambda t) \left(\int\limits_0^{2R} J(\lambda t') h(y,t') dt' \right) - J(\lambda t) \left(\int\limits_0^{2R} Y(\lambda t') h(y,t') dt' \right) \right] \lambda^{2n-3} d\lambda, \tag{20}$$

$$J(t) = \frac{J_{n/2-1}(t)}{t^{n/2-1}}, \qquad Y(t) = \frac{Y_{n/2-1}(t)}{t^{n/2-1}},$$

$J_{n/2-1}(t)$ and $Y_{n/2-1}(t)$ are respectively the Bessel and Neumann functions of order $n/2-1$, and $\mathbf{n}(y)$ is the vector of exterior normal to ∂B.

In 2-D equations (19), (20) can be simplified to yield the following reconstruction formula:

$$f(x) = -\frac{1}{2\pi^2} \mathrm{div} \int\limits_{\partial B} \mathbf{n}(y) \left[\int\limits_0^{2R} g(y,t') \frac{1}{|x-y|^2 - t'^2} dt' \right] dl(y).$$

A similar simplification is also possible in $3D$ resulting in the formula

$$f(x) = \frac{1}{8\pi^2} \mathrm{div} \int\limits_{\partial B} \mathbf{n}(y) \left(\frac{1}{t} \frac{d}{dt} \frac{g(y,t)}{t} \right) \Bigg|_{t=|y-x|} dA(y). \tag{21}$$

(Simultaneously, an essentially different set of inversion formulas for even dimensions were obtain in [8]). The straightforward discretization of these formulas leads to algorithms of complexity $\mathcal{O}(n^5)$ in 3-D and $\mathcal{O}(n^3)$ in 2-D. (Compare to the $\mathcal{O}(n^9)$ and $\mathcal{O}(n^6)$ complexity of the straightforward linear algebra approach). The application of these formulas make the computation feasible even in 3-D; the computation time for a grid of size $128 \times 128 \times 128$ is several hours. Some reconstruction results using these formulas are presented in ([3, 6, 7]).

3.2 Series solutions for arbitrary geometries

No explicit inversion formulas are currently known for the situation when the detectors are located on a non-spherical closed surface. We, thus, developed a different approach [4] that theoretically works for any closed S and that is practically useful in non-spherical geometries for which the eigenfunctions of the Dirichlet Laplacian are explicitly known. In particular, in the case of the cubic acquisition surface this approach leads to an extremely fast reconstruction algorithm.

Let λ_m^2 and $u_m(x)$ be the eigenvalues and normalized eigenfunctions of the Dirichlet Laplacian $-\Delta$ on the interior Ω of a closed surface S:

$$\begin{aligned} \Delta u_m(x) + \lambda_m^2 u_m(x) &= 0, \qquad x \in \Omega, \quad \Omega \subseteq \mathbb{R}^n, \\ u_m(x) &= 0, \qquad x \in S, \\ ||u_m||_2^2 \equiv \int\limits_\Omega |u_m(x)|^2 dx &= 1. \end{aligned} \tag{22}$$

As before, we would like to reconstruct a compactly supported function $f(x)$ from the known values of its spherical integrals $h(y,r)$ with centres on S:

$$h(y,r) = \int\limits_{\omega^{n-1}} f(y + r\omega) r^{n-1} d\omega, \qquad y \in S.$$

We notice that $u_m(x)$ is the solution of the Dirichlet problem for the Helmholtz equation with zero boundary conditions and the wave number λ_m, and thus it admits the Helmholtz representation

$$u_m(x) = \int_{\partial\Omega} \Phi_{\lambda_m}(|x-y|) \frac{\partial}{\partial \mathbf{n}} u_m(y) ds(y) \qquad x \in \Omega, \tag{23}$$

where $\Phi_{\lambda_m}(|x-y|)$ is a free-space rotationally invariant Green's function of the Helmholtz equation (22).

The eigenfunctions $\{u_m(x)\}_0^\infty$ form an orthonormal basis in $L_2(\Omega)$. Therefore, $f(x)$ can be represented by the series

$$f(x) = \sum_{m=0}^{\infty} \alpha_m u_m(x) \tag{24}$$

with

$$\alpha_m = \int_\Omega u_m(x) f(x) dx.$$

Since $f(x) \in C_0^1$, series (24) converges pointwise. A reconstruction formula of α_m, and thus of $f(x)$, will result if we substitute representation (23) into (24) and interchange the order of integration. Indeed, after a brief calculation we will get

$$\alpha_m = \int_\Omega u_m(x) f(x) dx = \int_{\partial\Omega} I(y, \lambda_m) \frac{\partial}{\partial \mathbf{n}} u_m(y) dA(x), \tag{25}$$

where

$$I(y, \lambda) = \int_\Omega \Phi_\lambda(|x-y|) f(x) dx. \tag{26}$$

Certainly, the need to know the spectrum and eigenfunctions of the Dirichlet Laplacian imposes a severe constraint on the surface S. However, there are simple cases when the eigenfunctions are well known, and fast summation formulas for the corresponding series are available. Such is the case of a cubic measuring surface S (see [4]); the eigenfunctions u_m are products of sine functions:

$$u_m(x) = \frac{8}{R^3} \sin\frac{\pi m_1 x_1}{R} \sin\frac{\pi m_2 x_2}{R} \sin\frac{\pi m_3 x_3}{R},$$

where $m = (m_1, m_2, m_3)$, $m_1, m_2, m_3 \in \mathbb{N}$, and the eigenvalues are easily found as well

$$\lambda_m = \pi^2 |m|^2 / R^2.$$

Sum (24) is just a regular 3-D Fourier sine series easily computable by application of the Fast Fourier Sine transform algorithm. The algorithmic trick that allows one to calculate the coefficients α_m quickly consists in first computing integrals (26) on a uniform mesh in λ. This is easily done by a one-dimensional Fast Fourier Cosine transform algorithm, with $\Phi_\lambda(t) = \cos(\lambda t)/t$. The normal derivatives of $u_m(x)$ are also products of sine functions, this time two-dimensional ones. This, in turn, permits rapid evaluation of the integrals $\int_{\partial\Omega_i} I(y,\lambda) \frac{\partial}{\partial \mathbf{n}} u_m(y) dA(x)$ for each mesh value of λ, and for each one of the six faces $\partial\Omega_i, i = 1, ..., 6$ of the cube. Finally, the computation of α_m using equation (25) reduces to the interpolation in the spectral parameter λ, since the integrals in the right hand side of this equation have been computed for the mesh values of this parameter (not for λ_m). Due to the oscillatory nature of the integrals (26) a low order interpolation here would lead to inaccurate reconstructions. Luckily, however, these integrals are analytic functions of the parameter λ (due to the finite support of g). Hence, high order polynomial interpolation is applicable, and numerics yields very good results.

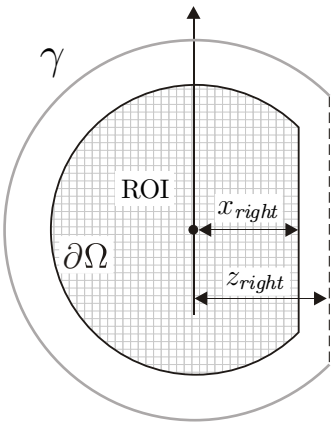

Figure 4: Geometry of the data acquisition

The algorithm we just described requires $\mathcal{O}(n^3 \log n)$ floating point operations if the reconstruction is to be performed on an $n \times n \times n$ Cartesian grid, from comparably discretized data measured on a cubic surface. In practical terms, it yields reconstructions in the matter of several seconds on grids with total number of nods exceeding a million [4]. This is a very significant improvement as compared to several hours of computation time required for the algorithms based on explicit inversion formulas (see previous section). No other known reconstruction method for TAT is capable of reconstructing images in a comparable time.

3.3 Reconstruction with detectors on an open curve

One of the open problems in TAT is reconstruction in the situation when the detectors can be placed only on a part of the surface surrounding the region of interest (ROI). Unfortunately, this is the case almost always, since the tomography scan of the whole body is almost never performed. We thus have developed [5] a quick non-iterative method that allows one to obtain qualitatively correct reconstruction in such situations. The method we present is currently working in 2-D, although extension to 3-D problems is possible.

In order to simplify the presentation we will concentrate on a truncated circular geometry as described below. The 2-D region of interest Ω is a truncated disk $\Omega(R, x_{right}) = \{x = (x_1, x_2) \mid x_1^2 + x_2^2 < R^2 \text{ and } x_1 < x_{right}\}$ and the centers of integration circles lie on the circular arch $\gamma(R_\gamma, z_{right}) = \{z = (z_1, z_2) \mid z_1^2 + z_2^2 = R_\gamma^2 \text{ and } z_1 < z_{right}\}$, where $R_\gamma > R$, see Figure 4. Our goal is to reconstruct a C_0^1 function $f(x)$ supported in Ω from the known values of its integrals $h(z, r)$ over circles $\mathbb{S}(r, z)$ of radii r centered at points $z \in \gamma$

$$h(z,r) = \int\limits_{\mathbb{S}(r,z)} f(x)dl(x) = r \int\limits_{\mathbb{S}^1} f(z + r\varpi)d\varpi.$$

In particular, we develop an efficient computational algorithm for the solution of this problem.

The present algorithm is based on precomputing the approximations of plane waves in Ω by the single layer potentials in the form $\int_\gamma Z(\lambda|z-x|)\rho(z)dl(z)$, where $\rho(z)$ is the density of the potential and $Z(t)$ is either the Bessel function $J_0(t)$ or the Neumann function $Y_0(t)$. Specifically, given a

wavevector ξ we find numerically the densities $\rho_{\xi,J}(z)$ and $\rho_{\xi,Y}(z)$ of the potentials

$$W_J(x,\rho_{\xi,J}) = \int_\gamma J_0(\lambda|z-x|)\rho_{\xi,J}(z)dl(z), \tag{27}$$

$$W_Y(x,\rho_{\xi,Y}) = \int_\gamma Y_0(\lambda|z-x|)\rho_{\xi,Y}(z)dl(z), \tag{28}$$

where $\lambda = |\xi|$, such that

$$W_J(x,\rho_{\xi,J}) + W_Y(x,\rho_{\xi,Y}) \approx \exp(-i\xi\cdot x), \quad \forall x \in \Omega, \tag{29}$$

Obtaining such approximations is not trivial; we discuss this issue in more detail in the next section. However, if the densities $\rho_{\xi,J}$ and $\rho_{\xi,Y}$ have been found for all ξ then function $f(x)$ can be easily reconstructed. Indeed, let us introduce convolutions $G_J(\lambda,y)$, $G_Y(\lambda,z)$ as follows

$$G_J(\lambda,z) = \int_\Omega f(x)J_0(\lambda|z-x|)dx,$$
$$G_Y(\lambda,z) = \int_\Omega f(x)Y_0(\lambda|z-x|)dx.$$

We notice that the boundary values of these functions for all $z \in \gamma$ can be computed from projections $g(z,r)$:

$$G_J(\lambda,z) = \int_{R^+} h(z,r)J_0(\lambda r)dr, \tag{30}$$

$$G_Y(\lambda,z) = \int_{R^+} h(z,r)Y_0(\lambda r)dr. \tag{31}$$

Consider now the Fourier transform $\hat{f}(\xi)$ of $f(x)$

$$\hat{f}(\xi) = \frac{1}{2\pi}\int_\Omega f(x)\exp(-i\xi\cdot x)dx.$$

Using (29) we obtain

$$\begin{aligned}
\hat{f}(\xi) &\approx \frac{1}{2\pi}\int_\Omega f(x)\left[W_J(x,\rho_{\xi,J}) + W_Y(x,\rho_{\xi,Y})\right]dx \\
&= \frac{1}{2\pi}\int_\gamma \left[\int_\Omega f(x)J_0(\lambda|z-x|)dx\right]\rho_{\xi,J}(z)dl(z) \\
&+ \frac{1}{2\pi}\int_\gamma \left[\int_\Omega f(x)Y_0(\lambda|z-x|)dx\right]\rho_{\xi,Y}(z)dl(z) \\
&= \frac{1}{2\pi}\int_\gamma \left[\rho_{\xi,J}(z)G_J(\lambda,z) + \rho_{\xi,Y}(z)G_Y(\lambda,z)\right]dl(z).
\end{aligned} \tag{32}$$

Formulas (30) and (31) in combination with (32) allow us to reconstruct (approximately) the Fourier transform $\hat{f}(\xi)$ of $f(x)$. Now $f(x)$ can be recovered by inverting the 2D Fourier transform. In order to minimize the operation count we will compute $G_J(\lambda,z)$ and $G_Y(\lambda,z)$ (using (30) and (31)) for a set of fixed values of $\lambda = |\xi|$; thus, the values of $\hat{f}(\xi)$ will be found on a polar grid in ξ. One can now use a high-order 2-D interpolation to obtain values of the Fourier transform on the Cartesian grid and apply the inverse 2D Fast Fourier Transform (FFT). Another approach is to utilize the famous slice-projection theorem (see, for example [10]) and reconstruct from the values of $\hat{f}(\xi)$ on the polar grid the regular Radon projections of $f(x)$; the function then can be obtained by the application of the FBP algorithm [10]. We have chosen the latter approach. The whole algorithm can be briefly outlined as follows.

1. Choose a uniform polar grid in ξ (the details are explained below). For each value of $\xi_{i,j} = \lambda_i(\cos\theta_j, \sin\theta_j)$ precompute $\rho_{\xi_{i,j},J}$ and $\rho_{\xi_{i,j},Y}$ as described in the next section. This step does not depend on values of $h(z,r)$ and needs to be performed only once for each particular geometry.

2. Given values of $h(z,r)$, compute $G_J(\lambda_i, z)$ and $G_Y(\lambda_i, z)$ (using (30) and (31)) for each value of i. This can be done using the trapezoid rule in r.

3. Compute $\hat{f}(\xi_{i,j})$ according to (32), using the same discretization of the integral as was used to obtain (27) and (28).

4. Apply 1-D FFT to values of $\hat{f}(\xi_{i,j})$ for each fixed j, to reconstruct the classical Radon projections of $f(x)$ corresponding to the angular parameter θ_j. (Alternatively, in the presence of strong noise in the data one can introduce a lower-pass filter $\eta(\xi)$ and use $\eta(|\xi_{i,j}|)\hat{f}(\xi_{i,j})$ instead of $\hat{f}(\xi_{i,j})$ on this step).

5. Use the well-know FBP algorithm [10] to reconstruct $f(x)$ from the standard Radon projections.

Suppose the size of the Cartesian reconstruction grid is $n \times n$, and s is the step of the grid ($s = 2R/(n-1)$). Assume for simplicity that the projections are discretized in r with the same step s. Then the highest spatial frequency one can hope to recover is the Nyquist frequency $\lambda_{\max} = \pi(n-1)/(2R)$. In turn, the Nyquist step $\Delta\lambda_{Nyquist}$ for the discretization in the frequency domain depends on the size of the support of the projections ($2R$); it equals π/R. We found that the better results are obtained if one uses step $\Delta\lambda$ half that size, i.e. $\Delta\lambda = \frac{1}{2}\Delta\lambda_{Nyquist} = \frac{\pi}{2R}$. In order to chose the number of wave propagation directions θ_j we recall that the optimal number of classical Radon projections for the FBP algorithm is $\pi n/2$ (see [10]), in the angular interval of size π. Thus, our uniform polar grid in ξ is discretized with step $\Delta\lambda$ from 0 to $\lambda_{\max}$ in the radial direction, and with step $2/n$ from 0 to π in the polar direction. There is no need to compute values of $\hat{f}(\xi_{i,j})$ for the values corresponding to the polar angle from π to 2π, since the function $f(x)$ is real-valued.

It is clear that the number of detectors (or the number of projections) should be of order $\mathcal{O}(n)$. We found in numerical experiments that the best results are obtained when this number is about 20% higher than πn. With such values of discretization parameters steps 2, 3, and 5 of the algorithm require $\mathcal{O}(n^3)$ floating point operations; step 5 is faster ($\mathcal{O}(n^2 \log n)$ flops). Step 1, described in the next section, is more expensive computationally. The precise operation count depends on the algorithm used to compute n Singular Value Decompositions (SVD) for matrices of size $(n \times n)$, and can be $\mathcal{O}(n^4)$ operations or higher. However, step 1 needs to be performed only once for each particular geometry. The number of data generated on step 1 and stored on a hard drive (values of the densities $\rho_{\xi_{i,j},J}$ and $\rho_{\xi_{i,j},Y}$) is of order $\mathcal{O}(n^3)$. The rest of the algorithm, including reading the precomputed densities, is completed in $\mathcal{O}(n^3)$ operations (similarly to the FBP).

Obviously, the feasibility of this method hinges on our ability to find approximations in the form (29). The existence, accuracy and stability of such approximations is discussed in detail in [5].

We demonstrate the performance of our method in the following numerical experiment. As a phantom (a simulated source of the acoustic wave) we used the sum of the characteristic functions of circles as shown in Figure 5(a). Part (b) of the latter figure demonstrates the image reconstructed from accurate projections (measurements of acoustic pressure). In order to analyze the sensitivity of the method to non-exact measurements we added to the projections white noise with intensity of 15% of the signal (in L^2 norm); the reconstruction is shown in Figure 5(c). As it is frequently done in tomography, in order to reduce the effects of noise one can apply a low-pass filter on

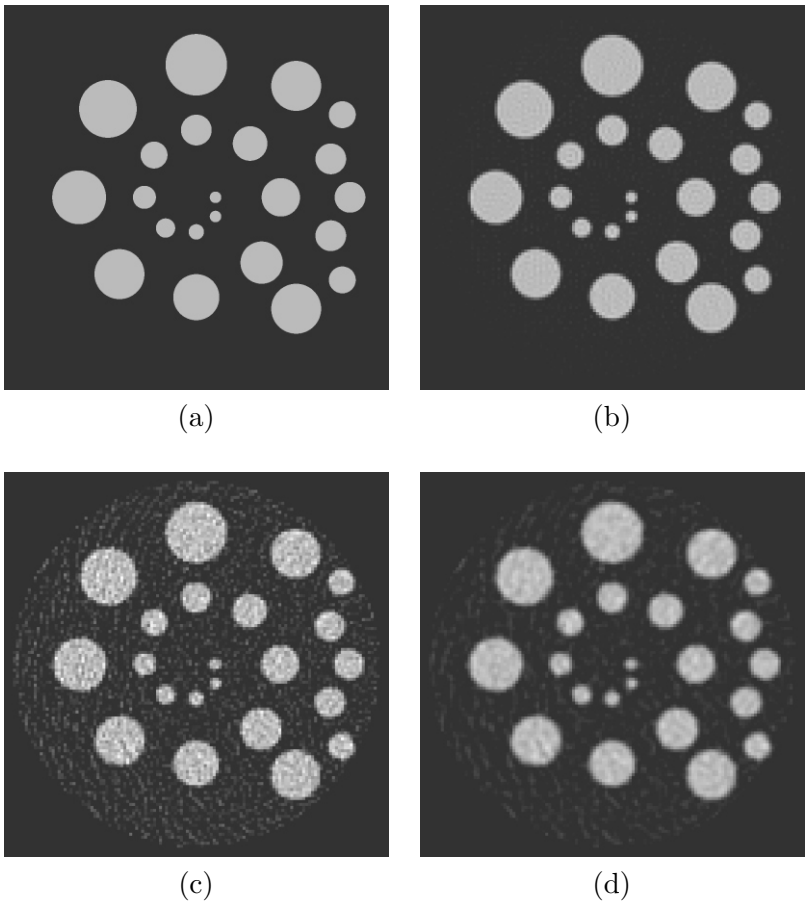

Figure 5: Geometry #1: (a) phantom, (b) reconstruction from the accurate projections (c) effect of 15% noise in projections (d) reconstruction from the noisy projections with the additional filter

step 4 of the algorithm. Part (d) demonstrates the effect of such additional filtration, with filter $\eta(\xi) = \cos(\frac{\pi}{2}|\xi|/\lambda_{Nyquist})$, where $\lambda_{Nyquist}$ is the Nyquist frequency of the reconstruction grid.

It should be noted, that if the densities $\rho_{\xi,J}(z)$ and $\rho_{\xi,Y}(z)$ have been precomputed, one reconstruction takes only about 4 seconds to compute; most of this time is spent on reading the values of the densities from the hard drive. The extension of this technique to 3-D is straightforward; however, we anticipate that precomputation of the densities will become time consuming, and, therefore, the development of a fast algorithm for such a calculation is required for a successful practical application of our method.

4 A broader impact

Besides purely mathematical results, this research effort also has had a broader impact. In particular, some parts of this projects have been implemented in collaboration with graduate students, which has enriched their research experience. While supported by the present grant, the PI co-organized AMS Joint Summer Research Conference in Mathematical Sciences *"Mathematical Modeling of Novel Optical Materials and Devices"*, Utah, Snowbird Resort, June 2005. The results of this research were disseminated by publication in the leading research journals, and through presentation on the following international conferences and symposia:

- Fast High-order Fourier/Chebyshev Methods for Large Eigenvalue Problems of Photonics, at minisymposium *"Light and Wave Propagation in Inhomogeneous Media: Theory and Modeling"*, SIAM Conference on Mathematical Aspects of Materials Science, LA. May 23-26, 2004.

- Inversion of the 3-D exponential parallel-beam transform by reduction to a set of the 2-D Radon transforms with angle-dependent attenuation, *AMS Special Session on Radon Transform and Inverse Problems*, Joint Mathematics Meetings, Atlanta, GA, January 5-8, 2005.

- Spectrally accurate Fourier methods in problems of wave propagation in inhomogeneous media, AMS Joint Summer Research Conference in Mathematical Sciences *"Mathematical Modeling of Novel Optical Materials and Devices"*, Utah, Snowbird Resort, June 2005.

- New reconstruction formulas and a fast algorithm for the inversion of 2-D circular Radon transform, Mathematical Methods in Tomography, Oberwolfach, Germany, July-August 2006.

- New reconstruction formulas and algorithms for problems of thermoacoustic tomography, 6th International Congress on Industrial and Applied Mathematics, ICIAM 2007, Zurich, July 2007. Minisymposium "Mathematical challenges in medical and industrial imaging".

- A series solution and a fast algorithm for the inversion of the spherical mean Radon transform, AIP 2007, Conference on Applied Inverse Problems 2007: Theoretical and Computational Aspects, Vancouver, June 25-29, 2007. Minisymposium "Mixed-mode medical imaging".

- Explicit inversion formulas for the spherical mean Radon transform, AIP 2007, Conference on Applied Inverse Problems 2007: Theoretical and Computational Aspects, Vancouver, June 25-29, 2007. Minisymposium "New topics in tomography".

- New reconstruction formulas and algorithms for problems of thermoacoustic tomography, Special Semester on Quantitative Biology analyzed by Mathematical Methods, Iohann Radon Institute on Computational and Applied Mathematics, Linz, Austria, 2007. Workshop "BioImaging I".

- Poster presentation: A simple, fast high-order solver for the problems of wave propagation in inhomogeneous media, OASCR Applied Mathematics PI Meeting, LLNL, Livermore, June 2007.

References

[1] L. Kunyansky, High-order accurate solution of 2-D eigenvalue problems of photonics, in preparation.

[2] L. Kunyansky, Fast, high-order accurate algorithms for computation of electromagnetic and acoustic scattering by penetrable objects, in preparation.

[3] L. Kunyansky, Explicit inversion formulas for the spherical mean Radon transform, *Inverse Problems*, **23** (2007), 373-383.

[4] L. Kunyansky, A series solution and a fast algorithm for the inversion of the spherical mean Radon transform, *Inverse Problems*, **23** (2007) s11-s200.

[5] L. Kunyansky, Thermoacoustic tomography with detectors on an open curve: an efficient reconstruction algorithm, *Inverse Problems*, **24** no. 5 (2008).

[6] M. Agranovsky, P. Kuchment, and L. Kunyansky, On reconstruction formulas and algorithms for the thermoacoustic and photoacoustic tomography, Ch. 8 to appear in L. H. Wang (Editor) *"Photoacoustic imaging and spectroscopy"*, CRC Press 2009.

[7] P. Kuchment and L. Kunyansky, A Survey in Mathematics for Industry: Mathematics of thermoacoustic tomography, *Euro. Jnl of Applied Mathematics* **19** (2008) 191–224.

[8] Finch, D., Haltmeier, M. & Rakesh 2007 Inversion of spherical means and the wave equation in even dimensions. SIAM J. Appl. Math. **68**, no 2, 392–412.

[9] Finch, D., Patch, S. & Rakesh 2004 Determining a function from its mean values over a family of spheres. SIAM J. Math. Anal. **35**, no. 5, 1213–1240.

[10] Natterer F 1986 *The Mathematics of Computerized Tomography*, Wiley.